

THE UNIVERSITY OF CHICAGO

MASTER'S THESIS

Generation and Characterization of Polarization Entangled Photon Pairs

Author:
Aditi GOYAL

Supervisor:
Dr. Cheng CHIN

*A thesis submitted in fulfillment of the requirements
for the degree of Master of Science*

in the

Physical Sciences Division

May 25, 2022

Abstract

Generation and Characterization of Polarization Entangled Photon Pairs

We experimentally demonstrate the generation of polarization entangled photon pairs at 852 nm. This infrared wavelength is the ^{133}Cs D_2 line, and the eventual goal with this experiment aims towards transferring the entangled photon pairs to Cs atoms. We use PPKPT crystal with phase matching for type-II SPDC. In our setup, we are utilising the bidirectionally pumping effectiveness of the Sagnac scheme by placing the crystal at the center of interferometer. Previous works have shown the advantages of the Sagnac loop with its higher stability and fidelity. For a 10 mW pump of 426 nm, we get 10,000 correlated down converted pairs. By changing the input pump state, we are able to prepare different states of entangled photon pairs. Currently, we achieve a $\sim 73\%$ purity with Bell state $|\psi^-\rangle$ pair. The entanglement of the state has also been characterized over different parameters and compared with Bell state parameters.

Acknowledgements

I am grateful to Prof. Cheng Chin for giving me the opportunity to join his lab, and to work on the entangled photons source project. I am sincerely thankful for his constant support, invaluable guidance and patience. Many discussions with Cheng helped me identify important aspects of the project. I learned many concepts of AMO physics and experimental techniques in the short span, for which I am thankful to the whole Chin group.

This thesis work wouldn't have been possible without Kevin (Kai-Xuan) Yao and Lauren Weiss, who taught me to work with optics in every step of the way. Thanks to Kevin for constructing the initial setup and helpful discussions whenever I was stuck. Thanks to Lauren for patiently answering many of my questions around optical components in the lab. Special thanks to Callum Welsh and Chang (Nick) Li for working on various components of the setup. I'd also like to acknowledge fruitful discussions with QMS lab members Jonathan Trisnadi and Mingjiamei Zhang.

Thanks to lab members and friends for reviewing my thesis.

Contents

Abstract	ii
Acknowledgements	iii
1 Introduction	1
1.1 Representation of Quantum States	1
1.1.1 Density Matrix Representation	2
1.1.2 Polarization States of Photons	2
1.2 Entanglement	3
1.2.1 Characteristics of Entangled States	4
1.3 Spontaneous Parametric Down Conversion	6
1.4 Correlated Photons	7
1.5 Optical Materials	7
2 Generation of Entangled Photon Pairs	9
2.1 Setup Design	9
2.1.1 Sagnac Interferometer	9
2.1.2 Crystal	10
2.1.3 Optical Components	10
2.1.4 Experimental Setup	11
2.2 Alignment	12
2.3 Electronics	14
2.3.1 Single Photon Counting Modules	14
2.3.2 FPGA	14
3 Characterization of Entangled Photon Pairs	15
3.1 Results	15
3.1.1 Tomography Results	17
3.2 Conclusion	19
Bibliography	20

Chapter 1

Introduction

Entanglement plays a key-role in applications of safe communication [15], cryptography [2], teleportation [6], and linear computation [12]. There have been many advances in generating the entanglement between photons [19], electrons [8], and molecules [18]. The scope of this thesis is around polarization entanglement in photon pairs.

The most common method to generate photon entanglement is via spontaneous parametric down conversion. In 1988, Shih et al.[7] and Ou et al.[27] demonstrated polarization entangled photons using type-I SPDC. In 1995, Kwiat et al.[19] showed entangling of polarization paired photons using a BBO crystal under type-II SPDC. Since then, many experiments have been performed to entangle photons using a non-linear crystal.

The Sagnac interferometer scheme for entanglement generation was first presented by Shi et al. [9] in which they noted good stability of output state even with perturbations. This work specifically draws inspiration from the experiments with a Sagnac configuration using a PPKTP crystal for type-II SPDC [25, 17]. The advantage of this scheme is that there is more stability in output phase of the photon pair state due to the special loop structure. Also, the bidirectional pumping yields more correlated photon pairs. In our experiment, we aim to generate entangled photon pairs at ^{133}Cs D_2 line, which is at 852nm.

When the entangled photons are to be transported for quantum application, it becomes crucial to characterize the entanglement. There are many parameters which characterize different measures of entanglement. Such parameters can be computed by performing a set of measurements, and reconstructing the quantum state through tomography.

We discuss the generation and characterization of entangled photons pairs in Chapter 2 and 3 respectively. In this chapter, we review the theoretical ideas which are cardinal to understanding the experiment.

1.1 Representation of Quantum States

Any single qubit state can be written as:

$$|\psi\rangle = \sum_i c_i |\phi_i\rangle, \quad \text{where } \sum_i c_i^2 = 1 \quad (1.1)$$

where, the set $\{|\phi_i\rangle\}$ forms an orthonormal basis in the Hilbert space H .

Similarly, a two qubit system can be represented as:

$$|\psi_{AB}\rangle = |\psi_A\rangle \otimes |\psi_B\rangle$$

1.1.1 Density Matrix Representation

Another way to represent a quantum state ensembles is through density matrices. It is useful to write the density matrix, in situations where the wavefunction is insufficient to describe the system. For instance, this situation may occur when the state is mixed, or after measurements have been performed on the system.

A density matrix is always positive, hermitian, and has unit trace.^[3] Generally, a density operator can be written as:

$$\hat{\rho} = \sum_i p_i |\phi_i\rangle \langle \phi_i|$$

where, the coefficients p_i are non-negative and add up to one.

Pure State

A state is said to be in a pure state when all the objects of an ensemble are in the same state. Then, the density matrix can be written as the outer product of the wavefunction. $\hat{\rho} = |\psi\rangle \langle \psi|$.

Example: The matrix form for a single qubit pure state:

$$\hat{\rho} = \begin{bmatrix} 1 & 0 \\ 0 & 0 \end{bmatrix}, \quad \hat{\rho} = |0\rangle \langle 0|$$

For a pure state, $\text{Tr}(\rho^2) = 1$

Mixed State

A mixed state density matrix cannot be decomposed into wavefunction. For a mixed state, $\text{Tr}(\rho^2) \neq 1$.

Example: The matrix form for a single qubit mixed state:

$$\hat{\rho} = \frac{1}{2} \begin{bmatrix} 1 & 0 \\ 0 & 1 \end{bmatrix}, \quad \hat{\rho} = \frac{1}{2} |0\rangle \langle 0| + \frac{1}{2} |1\rangle \langle 1|$$

1.1.2 Polarization States of Photons

An electromagnetic wave, such as light, has oscillating orthogonal electric and magnetic field components. Polarization can be understood as the direction of electric field of the light wave.

In $\{|H\rangle, |V\rangle\}$ basis, a single qubit polarization state can be written as:

$$|\psi\rangle = |H\rangle + e^{i\phi} |V\rangle \quad (1.2)$$

$|H\rangle$ and $|V\rangle$ stand for Horizontally and Vertically polarized light respectively. Polarization can also be represented in different bases, Diagonal, and Anti-diagonal, or Right circular light, and Left circular light, which are superposition states of $|H\rangle$, and $|V\rangle$.

$$\begin{aligned}
|D\rangle &= \frac{1}{\sqrt{2}}(|H\rangle + |V\rangle) \\
|A\rangle &= \frac{1}{\sqrt{2}}(|H\rangle - |V\rangle) \\
|R\rangle &= \frac{1}{\sqrt{2}}(|H\rangle + i|V\rangle) \\
|L\rangle &= \frac{1}{\sqrt{2}}(|H\rangle - i|V\rangle)
\end{aligned}$$

A two qubit polarization state can be written as:

$$|\psi_{AB}\rangle = |\psi_A\rangle \otimes |\psi_B\rangle$$

where, $|\psi_{A,B}\rangle$ is the wavefunction written as per eq. (1.2).

$$|\psi_{AB}\rangle = c_1 |H_A H_B\rangle + c_2 |H_A V_B\rangle + c_3 |V_A H_B\rangle + c_4 |V_A V_B\rangle \quad \text{where, } \sum_i |c_i|^2 = 1$$

For a mixed state, we have to write the density matrix:

$$\rho = \begin{matrix} & \begin{matrix} \langle HH| & \langle HV| & \langle VH| & \langle VV| \end{matrix} \\ \begin{matrix} |HH\rangle \\ |HV\rangle \\ |VH\rangle \\ |VV\rangle \end{matrix} & \begin{pmatrix} A_1 & B_1 e^{i\phi_1} & B_2 e^{i\phi_2} & B_3 e^{i\phi_3} \\ B_1 e^{i\phi_1} & A_2 & B_4 e^{i\phi_4} & B_5 e^{i\phi_5} \\ B_2 e^{i\phi_2} & B_4 e^{i\phi_4} & A_3 & B_6 e^{i\phi_6} \\ B_3 e^{i\phi_3} & B_5 e^{i\phi_5} & B_6 e^{i\phi_6} & A_4 \end{pmatrix} \end{matrix} \quad (1.3)$$

where, $\sum_i A_i = 1$ and A_i, B_i are real. This matrix is written using the hermiticity property of the density matrix.

1.2 Entanglement

Entanglement is a physical phenomena that occurs when two entities are correlated, such that if one entity is measured, accurate predictions can be made about the state of the other entangled entity.

Mathematically, it can be characterised in different ways. In the most simplistic way, for a pure state, entanglement can be defined when a quantum state cannot be written as a *product state*.

If a two qubit wavefunction can be separated like shown below, $|\psi_{AB}\rangle$ is said to be a product state.

$$|\psi_{AB}\rangle = |\psi_A\rangle \otimes |\psi_B\rangle$$

However, if it cannot be separated like this, it is said to be entangled. More generally, entanglement is better described by parameters of density matrix, which represents both pure and mixed states. This section contains a discussion of such parameters in the subsection 1.2.1.

Maximally entangled states

States which have maximum correlation with each other are maximally entangled. *Bell states* are maximally entangled for two qubits.

$$|\phi^\pm\rangle = \frac{1}{\sqrt{2}}(|00\rangle \pm |11\rangle)$$

$$|\psi^\pm\rangle = \frac{1}{\sqrt{2}}(|01\rangle \pm |10\rangle)$$

Another example of maximally entangled states are the *GHZ states* [11]. We can generalise them for n qubits:

$$|GHZ\rangle = \frac{1}{\sqrt{2}}(|0\rangle^{\otimes n} + |1\rangle^{\otimes n})$$

1.2.1 Characteristics of Entangled States

There are many methods to characterize entanglement of a system. Most of these methods are a direct result of density matrix. Below we explore the properties that characterize entanglement out of mixed states using density matrices.

Fidelity:

It is a characteristic that tells us about the overlap of the current state with any other chosen state. For pure state we can write:

$$F(\psi_1, \psi_2) = |\langle\psi_1|\psi_2\rangle|^2$$

However, for mixed states, we can only compute fidelity using the density matrices as per the below equation:

$$F(\rho_1, \rho_2) = (\text{Tr}(\sqrt{\sqrt{\rho_1}\rho_2\sqrt{\rho_1}}))^2$$

Generally, for characterizations, the overlap is done with maximally entangled Bell states. Higher the fidelity, higher the overlap with Bell state.

Entropy:

The entropy of entanglement is the Von-Neumann Entropy of the density matrix, and is similar to Gibb's or Shannon's entropy. Entropy characterizes the degree of mixture in quantum state. Higher the entropy value, higher the mixture.

$$S = -\sum_i \lambda_i \log(\lambda_i) \quad (1.4)$$

where, λ_i denotes the i^{th} eigen value.

For a pure state, entropy is 0. For a maximally mixed state, entropy is $\ln N$, where N corresponds to the dimension of Hilbert space.

There is one more variation to Entropy for characterizing the entanglement - *Linear Entropy*. Linear entropy is a result of making an approximation of $\ln \rho = \rho - 1$. This is usually easier to compute, and is given by:

$$S_L = 1 - \text{Tr}(\rho^2)$$

For a pure state, $S_L = 0$, for a completely mixed state, $S_L = 1$.

Concurrence:

The concurrence is another measure of entanglement, and it is estimated by the expression:

$$C(\rho) = \max(0, \lambda_1 - \lambda_2 - \lambda_3 - \lambda_4)$$

where, λ_i denotes the i^{th} eigen value of a matrix $R = \sqrt{\sqrt{\rho}\tilde{\rho}\sqrt{\rho}}$, with λ_1 being the highest eigen value. And, $\tilde{\rho} = (\sigma_y \otimes \sigma_y)\rho^*(\sigma_y \otimes \sigma_y)$, where ρ^* is the complex conjugate of ρ , and σ_y is the Pauli-y matrix.

Tangle:

It is another measure of non-classical property of a quantum state. It can be computed directly from the expression of Concurrence, $T = C^2$.

For a completely entangled state, $T = 1$.

It is particularly useful to differentiate between two entangled state on the basis of their entanglement, because it scales as C^2 .

Negativity:

This measure is a direct result of positive partial transposition criterion for a state [4, 16]. Generally, negativity is written as:

$$N(\rho) = \frac{||\rho^{T_B}|| - 1}{2}$$

where, $||\rho|| = \text{Tr}(\sqrt{\rho \dagger \rho})$ and, ρ^{T_B} is the partial transpose of ρ with respect to system B.

This estimate can also be computed from summing the negative eigenvalues of ρ^{T_B} i.e. the partial transpose of the density matrix .

$$N(\rho) = -\sum_i |\lambda_i|$$

Negativity reflects whether or not entanglement is present in the system. It is best to look at all 3 properties C, T, and N together when it comes to characterizing the entanglement.

Out of the above properties - Concurrence, Tangle, and Negativity are *entanglement monotonies* i.e. they quantify amount of entanglement present in a quantum state. These are more interesting and good way of characterizing entanglement, because the values of these functions do not increase with LOCC (local operations and classical communications) [13].

Let's see an *example* of the state,

$$|\psi\rangle = \frac{1}{\sqrt{2}}(|HV\rangle - e^{i\phi} |VH\rangle)$$

which is close to the Bell state pair $|\psi^-\rangle$. With this example, we want to analyse the density matrix, and discuss the entanglement properties for the state.

$$\hat{\rho} = |\psi\rangle \langle\psi|$$

$$\hat{\rho} = \frac{1}{2}(|HV\rangle - e^{i\phi} |VH\rangle)(\langle HV| - e^{-i\phi} \langle VH|) \quad (1.5)$$

$$\hat{\rho} = \frac{1}{2}(|HV\rangle \langle HV| + |VH\rangle \langle VH| - e^{-i\phi} |HV\rangle \langle VH| - e^{i\phi} |VH\rangle \langle HV|) \quad (1.6)$$

$$\hat{\rho} = \frac{1}{2} \begin{matrix} & \langle HH| & \langle HV| & \langle VH| & \langle VV| \\ \begin{matrix} |HH\rangle \\ |HV\rangle \\ |VH\rangle \\ |VV\rangle \end{matrix} & \begin{pmatrix} 0 & 0 & 0 & 0 \\ 0 & 1 & -e^{-i\phi} & 0 \\ 0 & -e^{i\phi} & 1 & 0 \\ 0 & 0 & 0 & 0 \end{pmatrix} \end{matrix} \quad (1.7)$$

We can diagonalize this matrix to find the eigenvalues. The eigenvalues are computed to be $\{1, 0, 0, 0\}$.

All the characteristics for entanglement can be written for this state as follows: Concurrence = 1, Tangle = 1, Von-Neumann Entropy = 0, Linear entropy = 0.

Eigen values of the partial transpose of the matrix = $\{-\frac{1}{2}, \frac{1}{2}, \frac{1}{2}, \frac{1}{2}\}$. Hence, Negativity = 0.5.

Fidelity is easy to compute for a pure state. On taking the inner product with $|\psi^-\rangle$, we can write $F = \cos^2(\frac{\phi}{2})$.

We will compare these results with our own tomography results for a similar state later in chapter 3.

1.3 Spontaneous Parametric Down Conversion

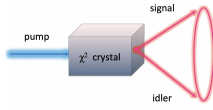


FIGURE 1.1: SPDC

When a pump photon passes through a non-linear optical crystal, the crystal produces two correlated photons of reduced frequencies. These are called Signal and Idler photons. These correlated photons travel along the edges of cones as show in figure 1.1 [1]. The down-conversion process refers to frequency down-conversion from input photons to output photon beams. Generally, the down-conversion efficiency is observed to be very low (of the order $\sim 10^{-4}$). SPDC is characterized to be of three types:

- Type 0: Down converted photons have the same polarization as the pump photon.
- Type I: Down converted photons have the same polarization, but are perpendicular to pump polarization.
- Type II: Signal and idler photons have perpendicular polarizations.

SPDC was first demonstrated in 1967 [24, 10]. Since then, many experiments have been performed to observe non-classical effects [23]. Predominantly, SPDC is easily used to generate entangled photons.

In our experiment, we carry out Type-II SPDC using a PPKTP crystal.

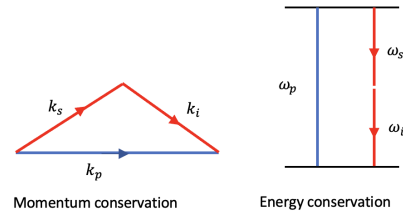


FIGURE 1.2: Phase Matching Conditions

Phase-Matching conditions

The phase matching-conditions are based upon energy and momentum conservation. We can write down the phase-matching equations to analyse the momentum and frequency of the downconverted beam from the pump beam or vice-versa.

$$\omega_p = \omega_s + \omega_i \quad (1.8)$$

$$\vec{k}_p = \vec{k}_s + \vec{k}_i \quad (1.9)$$

Figure 1.2 depicts the equivalence between total input \vec{k}_p and output momentum, also denoted by eq (1.9).

1.4 Correlated Photons

Co-incidences

The two photons - signal and idler are emitted from the crystal *simultaneously*. It is essential to being able to say that the emission is indeed simultaneous. This can be done by recording the two photon clicks at the same time, or by receiving both photon clicks within a very small time window. These events are termed as *coincidences*, because they occur more often than any such random chance events.

The number of coincidences is a very good measure of correlation, and thereby reflects the efficiency of SPDC. A higher number of coincidence would imply a signal photon is being detected along with its twin idler. Against the noise, this number should be high enough to portray the spontaneous downconversion.

Entangled polarization photons pairs

A general polarization entangled state for two photons can be written as:

$$|\psi\rangle = |HV\rangle + e^{i\phi} |VH\rangle \quad (1.10)$$

where, ϕ is the relative phase between $|HV\rangle$ and $|VH\rangle$.

Projecting into different bases

An entangled state $|HV\rangle + e^{i\phi} |VH\rangle$; we can write the state into different bases $\{|D\rangle, |A\rangle\}$, and $\{|R\rangle, |L\rangle\}$

Below is an *example* of projecting into $\{|D\rangle, |A\rangle\}$ basis.

$$\begin{aligned} |HV\rangle + e^{i\phi} |VH\rangle &= \frac{1}{2}((|D\rangle + |A\rangle)(|D\rangle - |A\rangle) + e^{i\phi}(|D\rangle - |A\rangle)(|D\rangle + |A\rangle)) \\ &= \frac{1}{2}(|DD\rangle (1 + e^{i\phi}) + \frac{1}{2} |AA\rangle (-1 - e^{i\phi}) + \frac{1}{2} |AD\rangle (1 - e^{i\phi}) + \frac{1}{2} |DA\rangle (-1 + e^{i\phi})) \end{aligned}$$

The advantage of projecting into different basis is that one can find out the phase ϕ with measurements in different bases.

1.5 Optical Materials

Prior to moving on to the experimental setup, it is essential to review the working of some of the important materials which are utilized in this experiment.

Polarizing Beamsplitter

A PBS (fig. 1.3) splits an incoming light beam into two orthogonal directions based on their polarizations. A horizontal polarized light beam will be transmitted, whereas a vertically polarized light beam is reflected.

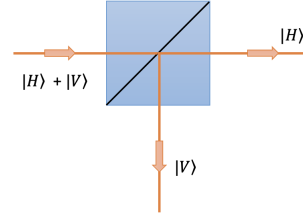


FIGURE 1.3: A PBS

Birefringence is an optical effect exhibited by non-linear optical materials. This effect is about dependence of the refractive index of the material on the characteristics of the input light beam, such as polarization and propagation direction of light.

Non-linear crystal

A good example of birefringent materials is a non-linear crystal, which essentially is the key component for down-conversion, second harmonic generation etc. The crystal follows the phase matching equations. We use a periodically poled crystal in our experiment. *Periodical poling* is the process of placing regular-spaced layers of alternate orientations of the non-linear material. This increases the efficiency of optical processes. This process provides a control over the range of wavelengths for which these certain processes occur. Periodically poled crystal ensures that *quasi phase matching conditions* will be followed [22].

$$\Delta k = k_p - k_s + k_i \pm 2\frac{\pi}{\Lambda} \quad (1.11)$$

where $k_j = 2\pi n_j / \lambda_j$

λ_j is the wavelength of input beam

n_j is the refractive index of crystal

Λ is the period of domain pattern inversion.

For any specific pump wavelength, and desired signal, idler wavelengths, the poling period can be computed using eq. (1.11).

Waveplates

Another example of a birefringent material is the waveplate. A waveplate works by introducing a phase shift in the light, i.e. by changing the polarization of the incoming beam. A controlled phase shift can be introduced depending on the incoming polarization, given its birefringent nature. Below is a review for QWP and a HWP.

A *quarter wave plate* works by converting a linearly polarized light into circularly polarized light. This happens by introducing different phase shifts to Horizontal and Vertical components, thereby making the wave circular/elliptical. The phase shift here is of $\pi/2$ between fast and slow axis components of the wave.

A *half-wave plate* introduces a phase shift of π between fast and slow axis components, and hence maintains the linearized polarization of the beam.

A combination of QWP, HWP and a PBS can be used to project the incoming beam into any other specific polarization. We will use this concept for projecting the beam into different polarizations while taking measurements.

Chapter 2

Generation of Entangled Photon Pairs

This Chapter describes the design and working of the setup. First there is discussion on optical setup, followed by alignment and electronic components.

2.1 Setup Design

Our experimental work of constructing the optical setup in a Sagnac scheme draws inspiration from previous works [25, 17]. The following section discusses the experimental setup (fig. 2.1(a)) and the optical components.

2.1.1 Sagnac Interferometer

A Sagnac interferometer is generally composed of two mirrors, and a PBS, in a loop like structure. The advantageous part of Sagnac scheme is that different polarizations from the PBS follow different paths (clockwise, and counter-clockwise), and then combine as one output from the PBS, yielding a high flux of output from the common path.

In our setup, further advantage is that we put the crystal in middle of two mirrors. The input pump goes through the crystal twice (clockwise, and counter-clockwise), this reduces the need for temporal compensation that usually becomes necessary in other photon entangled source experiments. This results in lower cost in generating entanglement. In 2004, Shi et al. [9] showed that the Sagnac setup also leads to a more stable structure with respect to output phase in the configuration.

As shown in fig 2.1(b) the beam-splitter splits the pump beam on the basis of their polarizations. The crystal only downconverts the $|H\rangle$ polarization beam as per phase matching eq. (1.11). This brings us to the idea of placing a half-waveplate in the path taken by vertical polarized pump towards the crystal. The waveplate is set to its slow axis, and brings a phase shift of $\pi/2$, i.e. $|V\rangle$ polarization turns into $|H\rangle$ polarization, and vice versa. The crystal converts the $|H\rangle$ polarization blue photons into red photons signal $|H_s\rangle$ and idler $|V_i\rangle$ simultaneously. The waveplate within the loop flips $|H_s\rangle |V_i\rangle$ into $|V_s\rangle |H_i\rangle$. The Beamsplitter will send $|V_i\rangle |H_i\rangle$ into path 1, and $|H_s\rangle |V_s\rangle$ into path 2. the biphoton state can be written as per eq. (2.1).

$$|\psi\rangle = |H_s\rangle_1 |V_i\rangle_2 + e^{i\phi} \beta |V_s\rangle_1 |H_i\rangle_2 \quad (2.1)$$

There can be a small phase ϕ because of the differences in two path lengths. Calculation about this phase has been done in detail by T. Kim et al. [25]. The factor of β depends on power ratio between the two clockwise and counter-clockwise pumps.

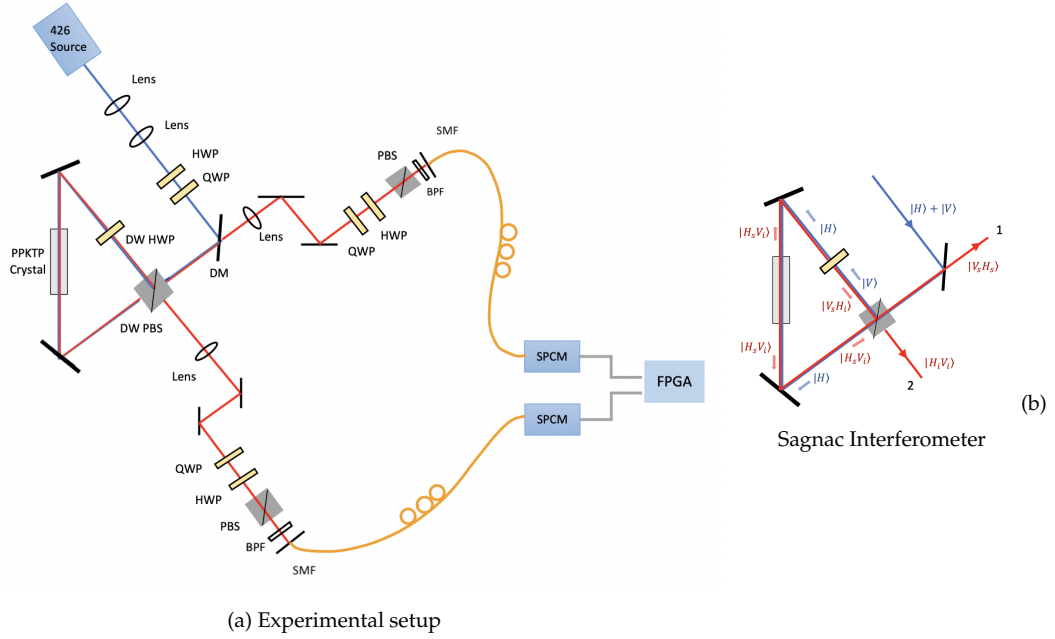


FIGURE 2.1: (a) The path taken by blue and red laser beam is traced. This is our full setup showing all components in the path. HWP, half-wave plate; QWP, quarter-wave plate; DM, Dichroic Mirror; BPF, band pass filter; SMF, single mode fiber; DW, dual wavelength, PBS, Polarizing Beam Splitter, (b) Polarization changes as the beam travels through the interferometer are depicted in the figure.

2.1.2 Crystal

We are using a PPKTP crystal (periodically poled potassium titanyl phosphate) from Raicol Crystals. The poling period for this crystal is 14.25 microns, and it is antireflection coated at 426 nm and 852 nm. The dimensions are $1 \times 2 \times 10$ mm. The optimal temperature was found to be 41°C . We use the Sellmeier equations to find out the refractive index of the crystal for some particular parameters of the beam. These parameters are temperature, wavelength, and polarization with respect to the axis of the travelling beam into the crystal [20]. For each axis, we have a different value of refractive index as per their input polarization.

Quasi-phase matching conditions are a fine approach to ensure that the crystal only down-converts the $|H\rangle$ polarization. This idea also helps when there are some imperfections with the cube. For example, let's say the beam-splitter reflects 3% $|H\rangle$ polarized beam. The quasi-phase matching conditions ensure that the 3% beam would not be down-converted.

2.1.3 Optical Components

We have used a Dual-Wavelength Polarizing Beamsplitter (PBS0012-405/810) of size $(12.7)^3$ mm, Dichroic mirror (DMLP650 nm from Thorlabs), Single-mode fibers (P5-780A-FC-2) with operating wavelength 780-970 nm, 850/10 nm BrightLine single-band bandpass filters. We use Thorlabs BB1E02 mirrors for blue beam, and place BB1E03 mirrors in the path taken by the red beam.

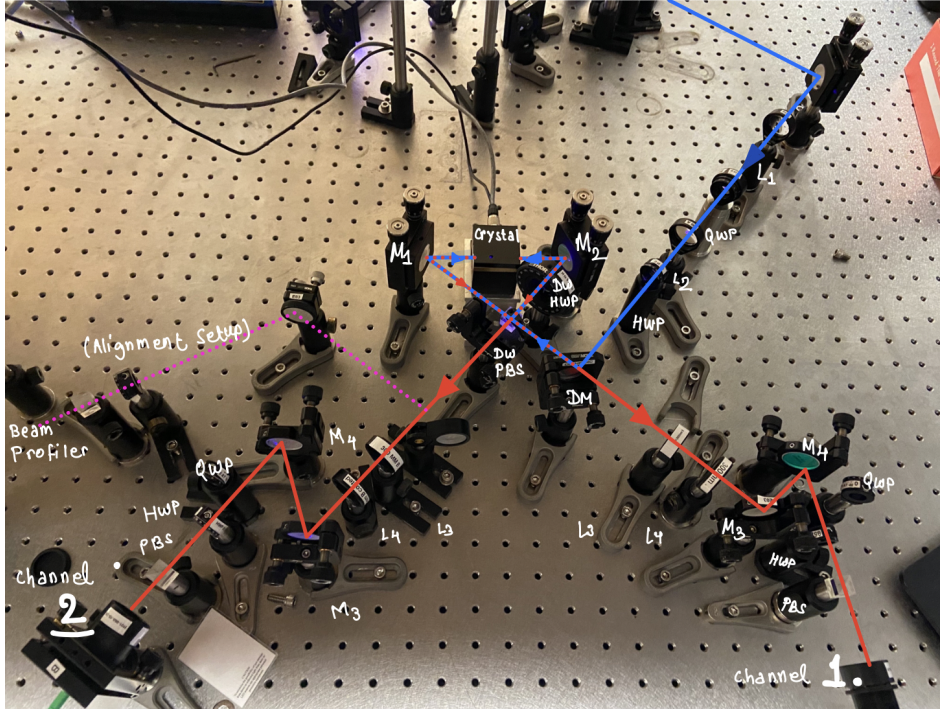


FIGURE 2.2: An image of our optical setup
The red and blue beam paths over the optical components.

2.1.4 Experimental Setup

We use a digital laser controller from Toptica Photonics which generates continuous wave 426 nm laser. We are using around 10 mW of blue laser power in our experiment. The 426 nm laser is coupled via single-mode fiber. Figure 2.2 shows the actual setup with blue beam originating out of the SMF, and reflecting off from a mirror towards the main setup.

There are lenses in the path to focus the beam at the crystal, and the DM reflects the blue pump into the Sagnac loop via DW-PBS. The *dichroic mirror* has a cutoff wavelength of 650 nm below which it reflects the beam, and above which it transmits. This is useful for our setup, as we use the dichroic to first reflect the blue light into Sagnac loop, and then transmit the red, which is tracing the same path, to go into the fiber detector.

The Sagnac loop has dimensions (10 + 15 + 10) cm. The output beams through the DW-PBS follow two paths as shown in figure 2.1(a). In the two paths, there are various components – beam focussing lenses, two mirrors for aligning each beam into each fibers, polarizer setups for tomography, and finally band pass filters.

The *band pass filters* do not allow any other wavelength of light apart from 850 ± 5 nm to pass through them, ensuring that the counts we obtain for our measurements are from down converted photons only.

Beam Focussing

To focus the beam, onto the crystal, a 50 mm and a 100 mm A coated lenses at 18 cm distance apart were placed. The beam waist at the crystal is ~ 1.1 mm. This distance was calculated for the given lenses using the Gaussian Beam Calculator software by Labview. It was observed that the change in the beam waist on the crystal from ~ 1.5 mm to ~ 1.1 mm, makes the coincidences to almost disappear (they go down

from 4000 to ~ 50). The downconversion effectiveness depends on the pump beam width at the crystal. This is the sharpest beam waist that we could attain with our available equipments along the crystal.

To focus the beam on the fiber-couplers, two 300 mm B coated lenses were used to tighten the beam waist at the lens of the fiber mount. These two lenses form a telescope structure, with the distance between the centre of the crystal and first lens, and the distance between the second lens and the fiber coupler being equal to 30 cm. This was a simple and quick way to restrict the beam waist at the fiber mount to be small, and roughly equal to the beam width at the crystal.

Furthermore, to ensure that the beam waist of the red beam going into the fibers is tightened as possibly as it could be, we have to take into account the lens at the fiber mount. One way to do this is to reverse pump in the 852 nm light through the fibers, and then change the beam waist at the crystal by changing the collimation of the fiber lens. One can use a spanner wrench to change the collimation of the fiber lens, such that the beam waist of reverse-pumped red at crystal is smallest possible.

Tomography setup

To perform tomography and record measurements, a polarizer analyzer form of setup is placed in each arm. Each setup is composed of a QWP, a HWP, and a PBS. This is to project the output beams into different polarizations.

2.2 Alignment

There are two main challenges that were faced in terms of alignment. The first one was getting coincidences between two channels. We were getting high number of counts in each channel, but no coincidences. There are many aspects that helped solving this problem - efficient beam focussing, and traversing the beam using the tip-tilt knobs on the fiber mounts. We already discussed about beam focussing, let's see why traversing the beam helps in this situation. As shown in fig 2.3, the coincidences and entanglement under SPDC occur at the highlighted points in black - where the two orange circles intersect in the horizontal line with the pump photon. In the situation when we are looking at some other points on the circle, but not highlighted points, we might not get good coincidences. The idea is to optimistically traverse along the circle in the search of the coincidences until we reach the highlighted points.

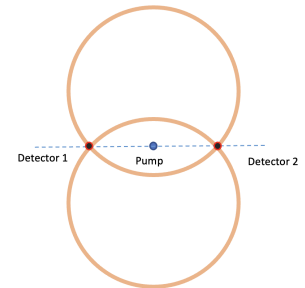


FIGURE 2.3: SPDC cones for signal and idler photons. The highlighted black points denote the location where entanglement occur [1].

The second one is aligning the two output beams coming from Sagnac loop's PBS precisely into the fibers. Since the fibers are extremely sensitive to the position of the beam (on the scale of μm), it becomes necessary to align the two clockwise and the counter-clockwise beams effectively. If they are not aligned fully, the peak photon counts for each beam occur at two different spatial positions. As a result of which, we end up looking at counts and coincidences for only one beam, instead of utilizing the bidirectional pumping effectiveness of the Sagnac loop.

To align the two output beams, we use the concept of interference. When two beams

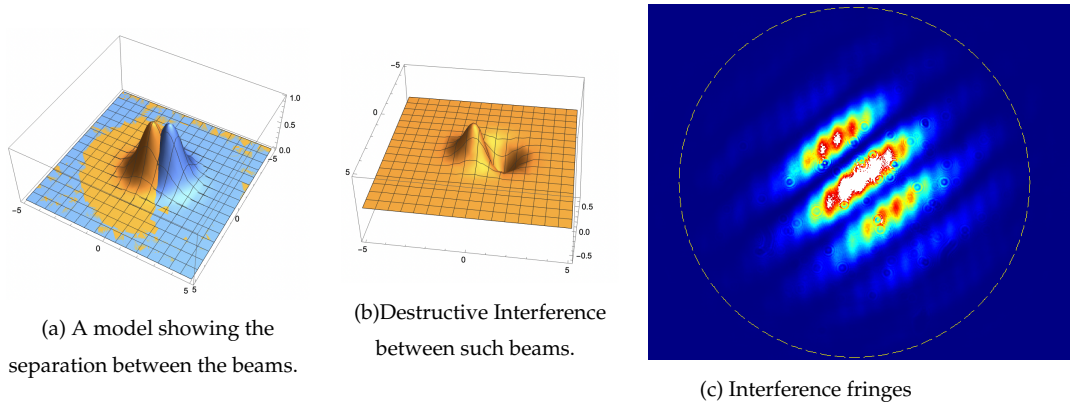


FIGURE 2.4: Two Gaussian Beams Spatially Separated

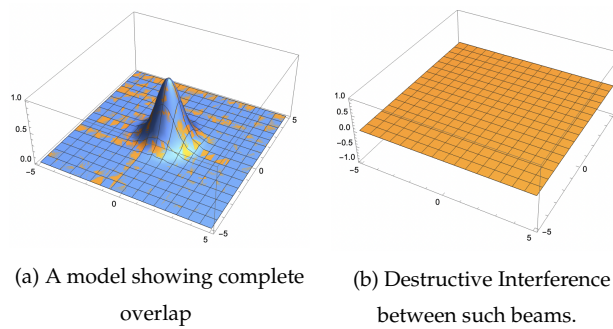


FIGURE 2.5: Two Gaussian beams in perfect alignment

are overlapping partially, but not aligned onto each other, they produce interference fringes. Such an example is modelled in fig. 2.4. Fig 2.4 (a) displays two Gaussian beams which are not in full alignment, and (b) displays the destructive interference of the two beams.

To interfere, the two beams should be of the same polarization to interfere i.e. the fields will add up constructively or destructively, only when they are in same direction. Hence, we construct a polarizing setup consisting of a HWP, and a PBS, and we place the beam profiler to look at the interference. As an example, the fig 2.4(c) was taken for interference after projecting both equal powered beams into anti-diagonal polarization, and this displays the fringes as we expect in the said situation.

To change the position of beams, we rotate the horizontal and vertical knobs iteratively on the interferometer mirrors to walk the two beams closer together until the pattern begins to resolve into a Gaussian beam. For destructive interference, we should observe no beam at all for a balanced power setup. This case is modeled in fig 2.5. Aiming to get no pattern at all when balanced beams are interfering would be an absolute way to ensure that the beams are fully aligned, as elaborated by fig 2.5(b).

We aim to align the setup through this method at two distanced positions to make sure the beams are aligned throughout. Currently, we are able to align at one position, but not at both positions. This does not result in an optimal result that we would rather expect, but we are progressing towards it by exploring more ideas.

2.3 Electronics

In order to make and record measurements, we need precise electronics. The following section details about the working principles of the electronics used in this experiment.

2.3.1 Single Photon Counting Modules

Since the down converted signal is too low to be detected by a usual Spectrometer or a power meter, there is a need to use a device which is sensitive to photon counts. For this purpose, a special class of photodetectors - SPAD's (Single-photon Avalanche Diode) can be used. They can detect low intensity signals and signal the time arrival of photons sensitively. SPAD's are based on Avalanche breakdown effect, which operate on reverse biased p-n junction above the breakdown voltage. They are capable of registering the photo-current of even a single photon.

We use the COUNT-NIR-50 modules from Laser Components. These counters are advertised with a 50% photon detection efficiency at 852 nm. This module outputs a 3V TTL pulse lasting 30 ns when it detects an incoming photon.

2.3.2 FPGA

We use a Xylo-Em FPGA board, along with NIST's software and firmware, which detects pulses, and generates real-time data of counts from each channel and coincidences. We build the user interface of time tagging with Labview software. We can observe the graph of counts vs. time elapsing for each channel in real-time on the LabView front panel.

For a particular time bin (20 ns), if there occurs a leading edge on both the detectors corresponding to a photon click, we consider it to be a coincidence. To find the coincidences, we do an 'AND' operation on the counts from each channel in these time windows on the LabView interface. The 20.8 ns time window is based on FPGA's internal clock, which is 48 MHz. The user interface displays counts per second, coincidences per second. We look at coincidences averaged over 10^7 points to look at a more stable coincidence number.

Chapter 3

Characterization of Entangled Photon Pairs

At the end of Chapter 2, we talked about taking measurements i.e. observing photon counts for each channel, and recording coincidences per second using the Tomography setup. In this Chapter, we present measurement results from our experimental setup, and reconstruct the density matrix with quantum state tomography to compare the characterization parameters of entanglement with an ideal example.

Since this Chapter addresses experimental measurement data, let's first talk about the errors that may prevail in the experiment.

Errors

Any measurement and analysis done by a human is error-prone in many ways: misreading of result, imprecise waveplates settings, accidental arrival of photons in the same time window, inaccurate density matrix construction.

While many such mistakes can be avoided and reduced, there are some which are not possible to be eliminated to an absoluteness i.e. noise. This noise can be factored into our measurements and it is generally termed as *random coincidences*.

Random coincidences

Given the statistical nature of light, there can always be coincidences occurring randomly. When integrated over a large period of time, these random fluctuations can be seen as a constant number. This number can be computed using the counts on each channel. The random co-incidences can be thought to be proportional to the counts in each channel, and inversely related to the time window. We use the below equation to compute the random co-incidences and we get $\sim (250 \text{ to } 500)$ coincidences occurring randomly in the setup.

$$\text{Random co-incidences per second} = \frac{\text{Count}_1 * \text{Count}_2}{48\text{MHz}}$$

3.1 Results

Counts on each channel

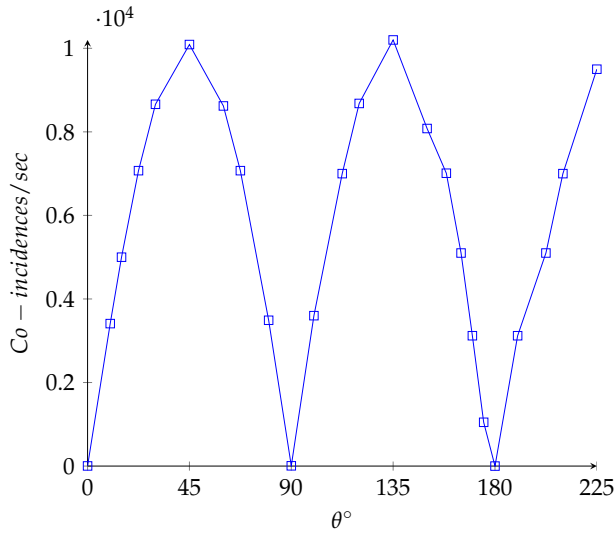
To get any counts, the first step is to align the beams into fibers with optimal precision. For this purpose, the two mirrors M_3 and M_4 (as shown in fig 2.2) can be used to change the position and angle of the beam going into the fiber respectively. The procedure is to walk the beam systematically using these two mirrors until the

highest optimal number of counts can be observed. The following results are for an almost balanced pump power between clockwise and counter-clockwise paths.

The maximum photon counts that we get are 210,000 and 116,000 for channel 2 and 1 respectively (Channels are annotated on fig 2.2). We get a maximum coincidences of 10,000 per second for a 10 mW power. This denotes an efficiency in terms of coincidences per each photon click, is around less than 10%. The coincidence numbers are obtained after subtracting the random coincidences, which are ~ 500 per second for maximum efficiency.

The following plot depicts the variation of coincidences per second with change in angle of the HWP in the tomography setup. The HWP in one of the two arms is kept at 0° , and HWP in the other arm is rotated, and the coincidence measurements are shown as data points in the plot. The data points imply that when both HWP's are set to project the beam into the state $|HH\rangle$, or $|VV\rangle$, the coincidences are negligible. This is in line with our expected state (eq. (2.1)).

This plotted data corresponds to real coincidences, obtained after subtracting the random coincidences. The plot can be modeled roughly as a sinusoidal wave with more number of accurate measurements.



With this data, however, we do not get a good entanglement with maximum optimised efficiency of one beam. The reason is due to the small spatial difference between two output beams, making the optimized alignment different for two different beams.

Hence, we perform a tomography with a data which has fewer coincidences than this, and we discuss the results in later section of this chapter.

Quantum State Tomography

Different parameters of characterizing entanglement are a result of density matrices, as discussed in Chapter 1. Hence, in order to find the measure of entanglement, it becomes imperative to construct the density matrix properly. Quantum tomography is the process of reconstructing the density matrix from measurements taken in different projections.

The general idea of Tomography is sketched below briefly:

Considering a two qubit density matrix, $\rho_{AB} = |\psi_{AB}\rangle \langle \psi_{AB}|$

We want to find a set Kraus operators $\{E_i\}$ for the operation $\epsilon(\rho)$ takes place as: $\epsilon(\rho) = \sum_i E_i \rho E_i^\dagger$ where, $\sum_i E_i^\dagger E_i = I$. We write the operators $\{E_i\}$ using another fixed set of operators, which form a basis and are based on experimental measurements made on the system. Plugging $\{E_i\}$ back in the above expression for $\epsilon(\rho)$, we get a χ matrix representation – which can be determined experimentally. We can find the operation, and the Kraus operators from χ , and thereby estimate the state ρ . This process is discussed in more detail in [3, 5].

Quantum process tomography also underlines a sufficient number of measurements that one may want to do to reconstruct the state.

Tomography Measurements

To perform a tomography, the idea is to project the polarization of down-converted beams into sufficient different bases from which, the density matrix can be reconstructed. For our experiment, measurements in $\{|H\rangle\}$, $\{|V\rangle\}$, $\{|D\rangle\}$, and $\{|R\rangle\}$ basis are sufficient. The $\{|H\rangle\}$, $\{|V\rangle\}$ basis may be considered as the computational basis, and both $\{|D\rangle\}$, and $\{|R\rangle\}$ form one component each from the other two bases. If we know $\{|H\rangle\}$, $\{|V\rangle\}$ and $\{|D\rangle\}$ bases measurements, measurements for $\{|A\rangle\}$ basis can be estimated, and similarly measurements for $\{|L\rangle\}$ can be estimated with $\{|H\rangle\}$, $\{|V\rangle\}$ and $\{|R\rangle\}$ bases measurements. These 4 basis sets constitute a total of 16 measurements for the two down-converted beams. The goal is to reconstruct a density matrix which is of the general form eq. (1.3).

In our endeavour to get entanglement, we equally divide the pump power to be sent into Sagnac setup and expect to get the Bell state $|\psi^-\rangle$ or $|\psi^+\rangle$. Measurements data corresponding to the expected state $|\psi\rangle$ is put up below:

$$|\psi\rangle = |HV\rangle - e^{i\phi} |VH\rangle$$

We use Kwiat Quantum Information Group's Tomography Interface to realize the density matrix [21]. Their interface has an option to input 16 or 32 measurements done in different bases for 2 qubits. Their method to compute the density matrix is based on maximum likelihood technique [26]. Analytically, calculating the maximum likelihood state is quite difficult, hence a numerical search is optimized. They make use of Stokes vectors to parameterize the measurements. J.B. Altepeter et al. describe this tomography process estimation in detail [14].

3.1.1 Tomography Results

The tabulated data is an input to Kwiat's tomography interface. Their code returns the reconstructed density matrix which is:

$$\hat{\rho} = \begin{matrix} & \langle HH| & \langle HV| & \langle VH| & \langle VV| \\ \begin{matrix} |HH\rangle \\ |HV\rangle \\ |VH\rangle \\ |VV\rangle \end{matrix} & \begin{pmatrix} 0.0186 & 0.0272 - i0.0233 & 0.0131 - i0.0201 & -0.0181 - i0.0223 \\ 0.0272 + i0.0233 & 0.357 & -0.346 - i0.0735 & -0.0167 - i0.0835 \\ 0.0131 + i0.0201 & -0.346 + i0.0735 & 0.575 & 0.042 - i0.001 \\ -0.0181 + i0.0223 & -0.0167 + i0.0835 & 0.042 + i0.001 & 0.0484 \end{pmatrix} \end{matrix}$$

State	Coincidences/s
$ HH\rangle$	0
$ HV\rangle$	230
$ HD\rangle$	128
$ HR\rangle$	151
$ VH\rangle$	440
$ VV\rangle$	0
$ VD\rangle$	216
$ VR\rangle$	225
$ DH\rangle$	210
$ DV\rangle$	110
$ DD\rangle$	52
$ DR\rangle$	260
$ RH\rangle$	204
$ RV\rangle$	240
$ RD\rangle$	430
$ RR\rangle$	111

TABLE 3.1: The above table presents the coincidences per second measured for different projections.

An interesting aspect can be observed quickly – only $(|HV\rangle + |VH\rangle)(\langle HV| + \langle VH|)$ terms have significant and comparable amplitudes, and all the other terms in the matrix are of the order 10^{-2} . The above matrix is similar to the example (eq. 1.7) we discussed in Chapter 1. This is a good indication of entanglement, and suggests that our state displays an identifiable proximity to the Bell state pair $|\psi^\pm\rangle$. Second thing is that the off-diagonal terms have negative real amplitude, indicating that the state is indeed closer to $|\psi^-\rangle$.

The Kwiat tomography portal also displays an histogram for the real and imaginary amplitudes of the density matrix as shown below in fig. 3.1.

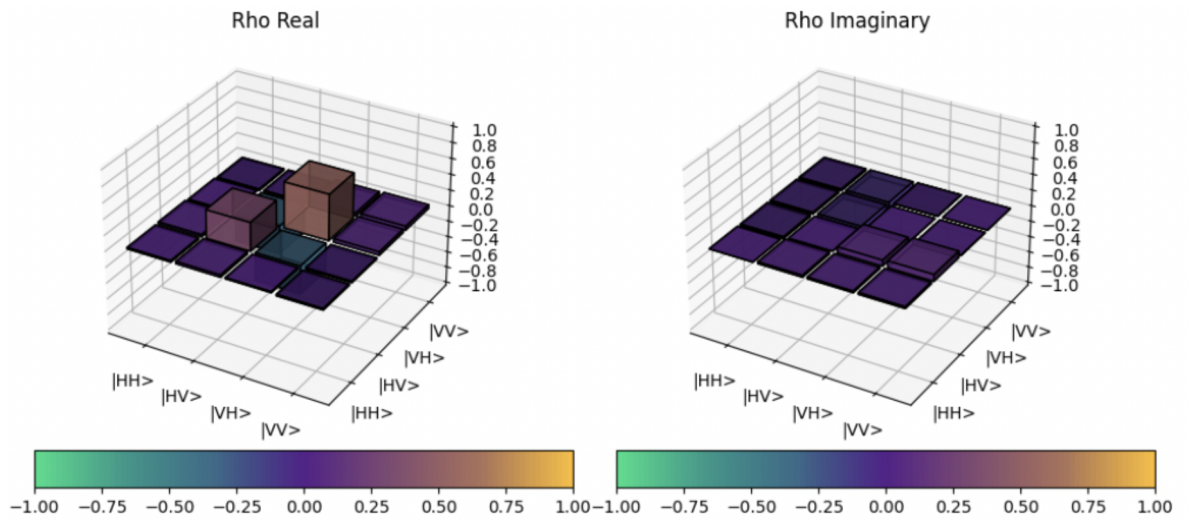


FIGURE 3.1: Reconstructed density matrix displayed as a histogram for real and imaginary amplitudes on the Kwiat tomography portal.

Characterization

The eigen values for this matrix are: $\{0.844, 0.156, 0, 0\}$.

We can now compute all the parameters of characterization for this state as we have discussed in Chapter 1.

I compute the fidelity of this state with Bell state $|\psi^-\rangle$ on Mathematica, and the fidelity results in a value $= 0.708 \sim \frac{1}{\sqrt{2}}$.

The other characteristics are computed with Kwiat tomography interface code.

Entanglement parameter	Experimental Computation	Ideal Estimate
Concurrence	0.74	1
Tangle	0.547	1
Entropy	0.624	0
Linear entropy	0.263	0
Negativity	0.66	0.5
Purity	0.736	1

TABLE 3.2: The table presents the different parameters of entanglement compared with the experimental computations and ideal estimate as per the example in the section 1.2.1.

The values of entanglement properties show decent entanglement, with acceptable values for concurrence, and tangle. However, the state is much more mixed than expected, as can be observed from the entropy value. Overall, the estimates show good signs of polarized entangled photon pairs.

3.2 Conclusion

We demonstrated the generation of entangled photon pairs with our Sagnac interferometer setup. We discussed the design and working of our setup, and components involved. The system downconverts around 10k correlated photons. With our results, we show that polarized entangled photon pairs are generated with type-II phase matched PPKTP under a Sagnac scheme. The resulting states display a fidelity closer to the Bell state $|\psi^\pm\rangle$.

Future works:

The tomography that we currently perform is based on finding a middle point where the two output beams are going into fibers equally. There can be more optimizations to align the setup better. We aim to continue the alignment to get good fidelity on our entangled state.

Bibliography

- [1] C. Couteau. In: *Contemporary Physics* 59(3), 291-304 (2018).
- [2] A.K. Ekert. In: *New J. Physics* 4, 47 (1991).
- [3] M.A. Nielsen and I. Chuang. In: *Quantum Computation and Quantum Information*, Cambridge Univ. Press (2000).
- [4] Asher Peres. In: *Physical Review Letters*. 77 (8): 1413–1415 (1996).
- [5] J. Preskill. In: *Lecture Notes on Quantum Computation* (1997-2015).
- [6] J.H. Shapiro. In: *Phys. Rev. Lett.* 67, 661 (2002).
- [7] Y. H. Shih. In: *Phys. Rev. Lett.* 61, 2921-2924 (1988).
- [8] B. Hensen *et al.* In: *Nature*, 526 (2015).
- [9] B. S. Shi *et al.* In: *Phys. Rev. A* 69, 013803 (2004).
- [10] D. Magde *et al.* In: *Physical Review Letters*. 18 (21): 905–907 (1967).
- [11] D.M. Greenberger *et al.* In: *Going Beyond Bell's Theorem*, FTPH, v37 (2007).
- [12] E. Knill *et al.* In: *Nature* 409, p46–52 (2001).
- [13] G. Vidal *et al.* In: *J.Mod.Opt.* 47 (2000) 355 (2000).
- [14] J.B. Altepeter *et al.* In: *Advances In Atomic, Molecular, and Optical Physics* v52 (2005).
- [15] L.-M. Duan *et al.* In: *Nature* 414, p413-418 (2001).
- [16] M. Horodecki *et al.* In: *Physics Letters A*. 223 (1–2) (1996).
- [17] Neng Cai *et al.* In: *Journal of the Optical Society of America B*, vol. 39 (2021).
- [18] Olaf Nairz *et al.* In: *American Journal of Physics*, 71 319–325 (2003).
- [19] P.G. Kwiat *et al.* In: *Phys. Rev. Lett.* 75, 4337 (1995).
- [20] P.J. Tsai *et al.* In: *Quantum Sci. Technol.* 3 034005 (2018).
- [21] P.S. Kuo *et al.* In: *Advances in Imaging and Electron Physics* v128, p205-308 (2003).
- [22] P.S. Kuo *et al.* In: v9762, *Advances in Photonics of Quantum Computing, Memory, and Comm.* IX (2016).
- [23] R. Ghosh *et al.* In: *Phys. Rev. Lett.* 59 (17): 1903–1905 (1987).
- [24] S.E. Harris *et al.* In: *Physical Review Letters*. 18 (18): 732–73 (1967).
- [25] Taehyun Kim *et al.* In: *Physical Review A* 73, 012316 (2006).
- [26] Z. Hradil *et al.* In: *Quantum State Estimation*, LNP v649, p59-112 (2004).
- [27] Z. Y. Ou *et al.* In: *Phys. Rev. Lett.* 61, 50-53 (1988).